

Mapping the continuity of the Nazca Plate through its aseismic part in the Arica Elbow (Central Andes)

Catherine Dorbath

ORSTOM and EOPG, URA 1358 CNRS, Paris, France

Received 13 March 1996; accepted 14 June 1996

Abstract

Along the Peru–Chile trench, the subduction of the Nazca Plate under South America is well underlined by the Wadati Benioff zone. In the Central Andes, the seismicity defines a moderately deepening slab down to about 325 km. The occurrence of a scarce seismicity in the 550–650 km depth range, after a complete seismic quiescence, raises the question of the continuity of the slab. To answer this question we performed a 3-D teleseismic tomography of the mantle at 20°S. On the tomographic image, a higher velocity zone is associated with the subducted plate where it is defined by the Wadati Benioff zone. At greater depth, this higher velocity body can be followed through the model down to the lower mantle. Our results provide clear evidence of the continuity of the slab throughout its seismically quiescent part. Moreover, they allow the imaging of the bending of the Nazca Plate in the Arica Elbow, where the general strike of the Andean chain changes and no deep seismicity has never been recorded. Finally, our results confirm the increase of the dip of the slab between 350 and 550 km in depth.

1. Introduction

The western part of South America is one of the major plate boundaries on the Earth. It is the largest region in which ocean–continent convergence is happening today. Moreover, it is the only region where an oceanic plate is subsiding under a major lithospheric plate and not under small continental blocks. The Andes are the result of the subduction of the Nazca Plate beneath the South American Plate along the Peru–Chile trench since the Cretaceous. This continental margin orogenic belt, continuous for more than 7000 km, presents distinct broad-scale tectonic segments; their coincidence with the varia-

tions in the geometry of the subducted Nazca Plate is very close (Barazangi and Isacks, 1976; Jordan et al., 1983). The most noticeable of these segments is certainly the Central Andes (15°S to 27°S): the range is at its widest part (Bolivian Orocline) including the Altiplano–Puna high plateau and the general strike of the structures changes from N320°W to nearly NS (Arica Elbow) (Fig. 1).

The location of the Wadati Benioff zone provides the most common way used to map subducting lithospheres. Numerous studies concerning the seismicity and shape of the Nazca Plate have been carried out, using a compilation of data from international centres (Sykes and Hayes, 1971; Stauder, 1973,

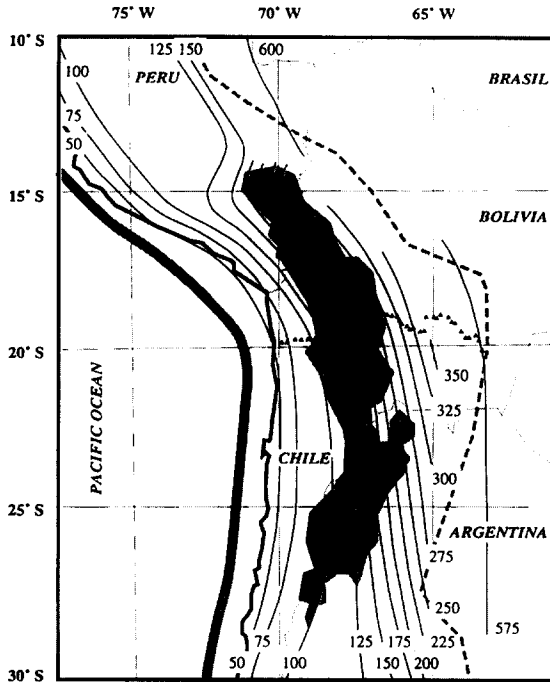


Fig. 1. Location map. The triangles represent the seismic stations of the 1994 Lithoscope experiment. The thick solid grey line off shore represents the Peru–Chile trench, and the dashed grey line inland the eastern limit of the Andean front of deformation. The pale grey zone represents the Altiplano, and the dark grey one Titicaca lake. The shape of the Nazca Plate is shown via contours to the depth of the centre of the Wadati Benioff zone from Cahill and Isacks (1992).

1975; Barazangi and Isacks, 1976, 1979; Bevis and Isacks, 1984). In the Central Andes, they describe the slab as continuously dipping to the east at a moderate angle of about 30° , and neighbouring segments (north of 15°S and south of 27°S) become nearly horizontal as they reach a depth of about 10 km. The updated compilation of Cahill and Isacks (1992) (Fig. 1) suggests that, in fact, this segment of the slab does not have a constant dip along its entire extent, but gradually flattens south of 20°S . Complementary data from local temporary networks operated in the same region support and refine the results obtained from teleseismic studies (Boyd et al., 1984; Grange et al., 1984; Comte and Suarez, 1995; Delouis et al., 1995). Whatever data, teleseismic or local, are used to map the geometry of the upper part of the subducted lithosphere, the downgoing plate is seismically defined in the Central Andes from the

trench down to 300–350 km. From this depth down to 500–550 km, a seismic quiescence is observed. Then few very deep earthquakes occur in clusters down to 600–650 km. Similar observations are made for the sub-horizontal subduction beneath central Peru, where the Wadati Benioff zone extends down to 100–125 km, then a seismic quiescence is observed down to 500 km, followed by a deep seismic zone. The lack of any events in the depth range 325–520 km is confirmed by the recent homogeneous and comprehensive catalogue produced by Kirby et al. (1995) who relocated 213 historical and modern deep events.

An important question arises: is the slab continuous or not through the aseismic zone? To answer this question we need to use techniques not based on mapping the local seismicity. In this way, Isacks and Barazangi (1973), Snoke et al. (1974) and Barazangi and Isacks (1976) studied the transmission through the region of anomalously high-frequency waves, but their results did not lead to any clear conclusion about slab continuity. Later on, models have been proposed suggesting either the absence of a slab in the aseismic zone (Wortel, 1982, 1984) or the continuity of the subducted plate (Engelbreton and Kirby, 1992). Recently, James and Snoke (1990) presented seismic evidence for the continuity of the Nazca Plate beneath central Peru ($10\text{--}14^\circ\text{S}$), in a segment where subduction becomes nearly horizontal. This result is based on the analysis of an anomalous P-wave arrival in the P codas of Peru–Brazil deep focus earthquakes recorded on the Carnegie broadband station at Cuzco. The authors concluded that the descending plate exists and is probably continuous, although aseismic, between 150 and 500 km depth, and is very steeply dipping (70°) below a depth of about 150 or 200 km. Finally, Engdahl et al. (1995) imaged the subducted lithosphere beneath South America by inversion of travel-time residuals of teleseismically well-recorded events that occurred in the region. Their study provides evidence for high-velocity material at depth and therefore for a probable continuity of the slab over regions with seismic quiescence. It also suggests that the slab penetrates the lower mantle.

In a recent paper (Dorbath et al., 1996), we provided corroborative evidence of the existence and continuity of the subducted Nazca Plate through the

aseismic zone beneath the Central Andes along a vertical cross-section at 20°S. This complementary paper will focus on the shape of the aseismic part of the slab below the Bolivian Orocline from 14 to 23°S, in the Arica Elbow region. These results are based on a 3-D tomography of the lithosphere down to a 660 km depth realized by the inversion of travel-time residuals of teleseismic P waves recorded during the 1994 Lithoscope field experiment. Such a method for mapping subducted lithosphere has never been used for the Nazca Plate. However, it has been used for other subduction zones, such as the western

Pacific (Hirahara, 1981) or eastern Pacific (Harris et al., 1991). Everywhere, slabs are evidenced by inclined high-velocity zones which well correlate with the Wadati Benioff zones (Hirahara and Hasemi, 1993). For western Pacific regions, which offer a large number of shallow, intermediate and deep focus earthquakes, local earthquake tomography offers a powerful complementary method to teleseismic tomography. Clearly, this assistance is not possible in our study area, as we intend to investigate an aseismic zone and very deep seismicity is scarce. On the other hand, the recent paper by Engdahl et al.

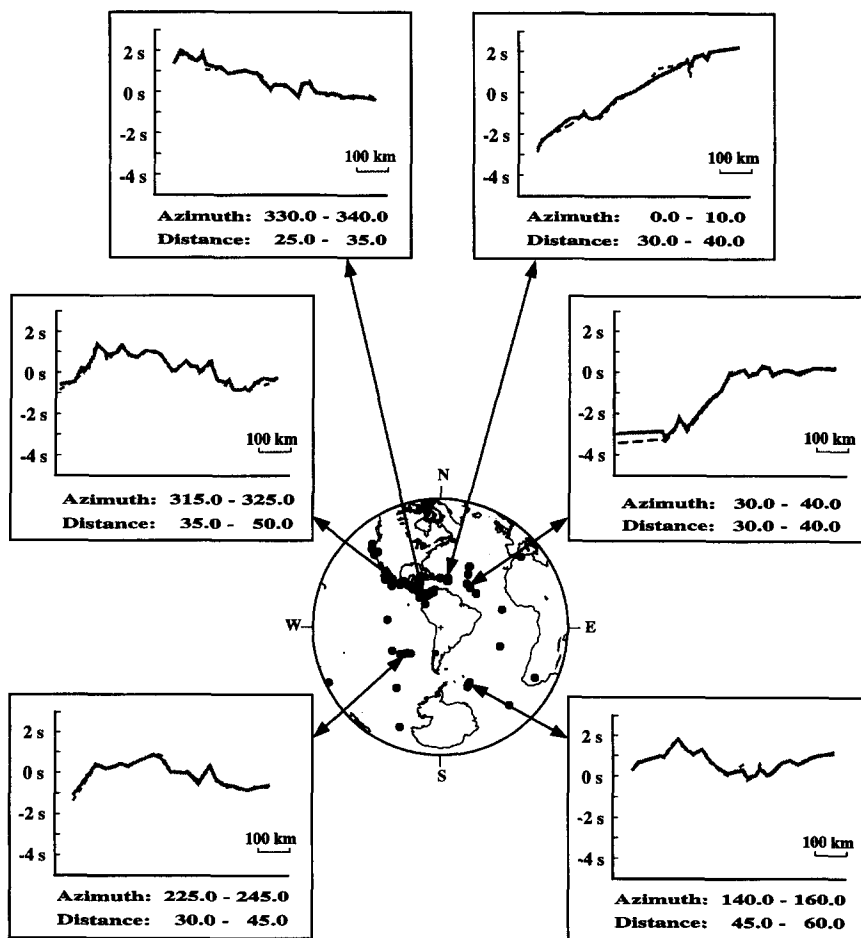


Fig. 2. Mean P residuals, relative to the same reference station located in the Altiplano, for six different epicentral regions. Dashed line, observed residuals; grey line, residuals computed using the final 3-D perturbation model obtained by the tomography. The map in the centre shows the distribution, relative to the centre of the Lithoscope array (black cross), of the events selected for the tomography at epicentral distances at less than 100°.

(1995) will provide a interesting basis for comparison: their large-scale tomographic image of the subducted Nazca Plate is obtained by inverting travel-time residuals of teleseismically recorded South American earthquakes and residuals at South American stations observed from events from a larger study region which includes the South Atlantic and eastern Pacific as well. Our tomographic image is obtained by inverting travel-time residuals of teleseismic events recorded on a local network; its scale, smaller in the upper layers, is of the same order of magnitude as Engdahl's study in the deeper layers.

2. Data

From June to November 1994, 41 vertical short-period stations from the French Lithoscope network were operated along a 700-km-long profile crossing the Andean chain in its entirety. Therefore, this profile was placed above the subducted plate from the coast, where the upper part of the plate is at a 50 km depth, to its eastern limit as it is defined by the Wadati Benioff zone; the profile ended at the sub-Andean front of deformation, above the very deep seismicity. The profile was designed to be as perpendicular as possible to the structures. The spacing between the stations was about 20 km (Fig. 1).

Among the 250 teleseismic events recorded during the 6-month experiment, we selected 120 events which provided clear P-wave arrivals at more than

ten stations. They were evenly distributed in distance and azimuth relative to the seismic network. Absolute travel times were calculated using hypocentral data from the USGS's Preliminary Determination of Epicenter's bulletin and Herrin's tables (Herrin, 1968). Next we calculated residuals at every station for every selected event, and then we computed the value of these residuals relative to the same reference station situated in the Altiplano. A study of the variation along the profile of these relative residuals was presented in a preliminary paper (Dorbath et al., 1996). However, we show again in Fig. 2 (dotted line) some P-wave residual profiles which are within the scope of this study.

To avoid errors due to poor readings or source peculiarity, we plotted profiles of mean relative residuals for some source regions, and not for singular events. Unfortunately, there is a lack of active seismic zones in the eastern and western azimuths, it is aligned with our linear network, which could provide direct and reverse profiles of residuals, and consequently help us to make simple qualitative modelling. Fig. 2 shows the strong azimuthal variations of P relative residuals and particularly the difference between the north-eastern quadrant and the other azimuths. For the azimuths between 0 and 40°E, the more we go west, the more the relative residuals are negative, therefore more rays cross high velocity structures. The decrease from east to west along the profile is more gradual for northern than for north-eastern azimuths, but on both profiles the

Table 1
Initial P-velocity model

Layer	Velocity (km s ⁻¹)	Thickness (km)	Nb of blocks N-S	Dimension (km)	Nb of blocks E-W	Dimension (km)
1	6.00	10	1	Cones	42	Cones
2	6.30	20	6	45	26	30
3	6.80	30	6	45	26	30
4	8.00	40	6	60	20	40
5	8.10	40	6	60	22	40
6	8.20	50	8	75	18	50
7	8.35	50	10	75	20	50
8	8.50	60	10	90	18	60
9	8.80	80	10	120	16	80
10	9.20	80	12	120	16	80
11	9.75	100	14	150	14	100
12	10.30	100	16	150	16	100

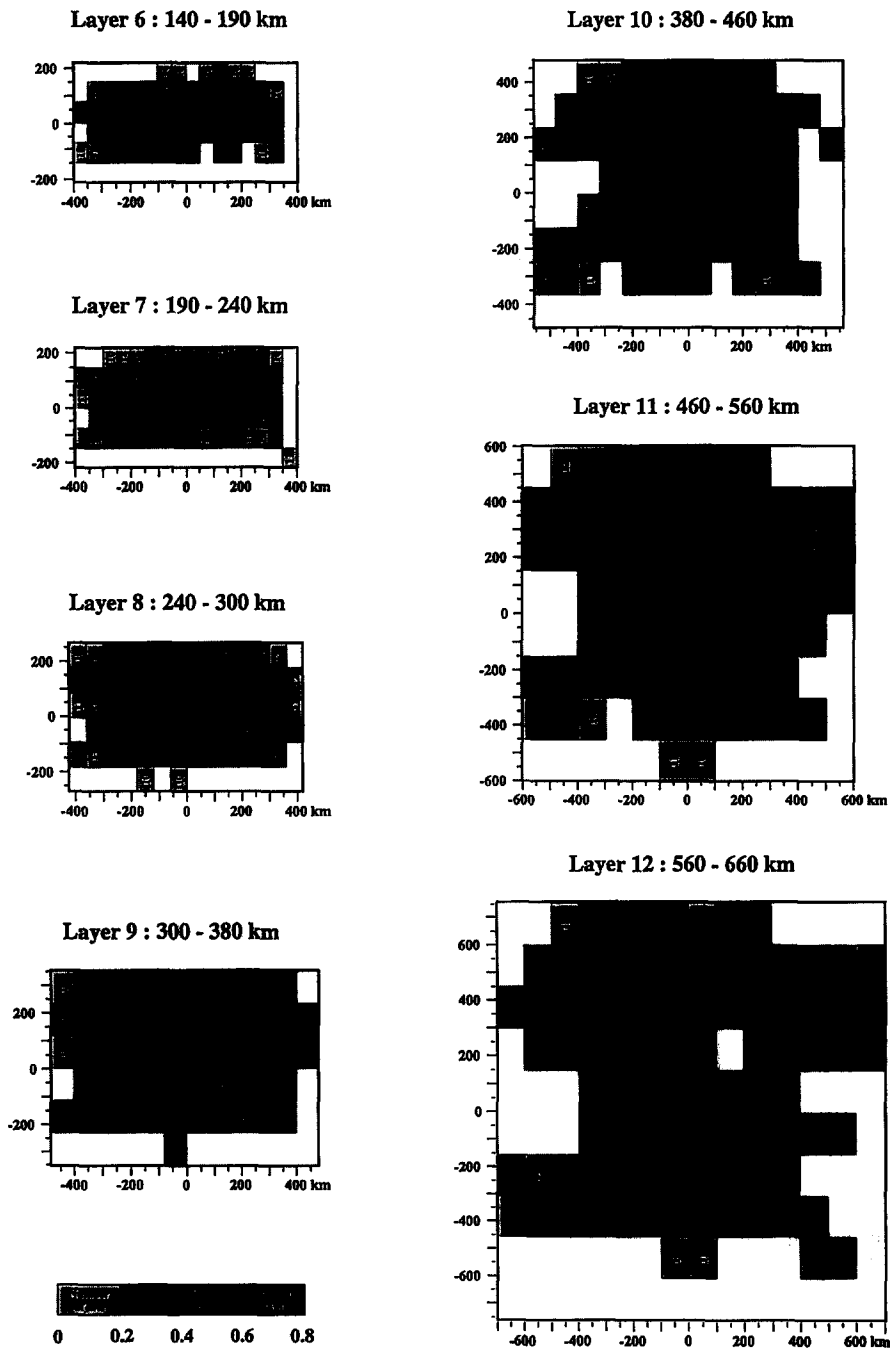


Fig. 3. Value of the diagonal element of the resolution matrix corresponding to each block in the seven deeper layers of the tomography. The darkest blocks are the best resolved in the inversion. The numbers indicate how many rays crossing each block were used in the inversion.

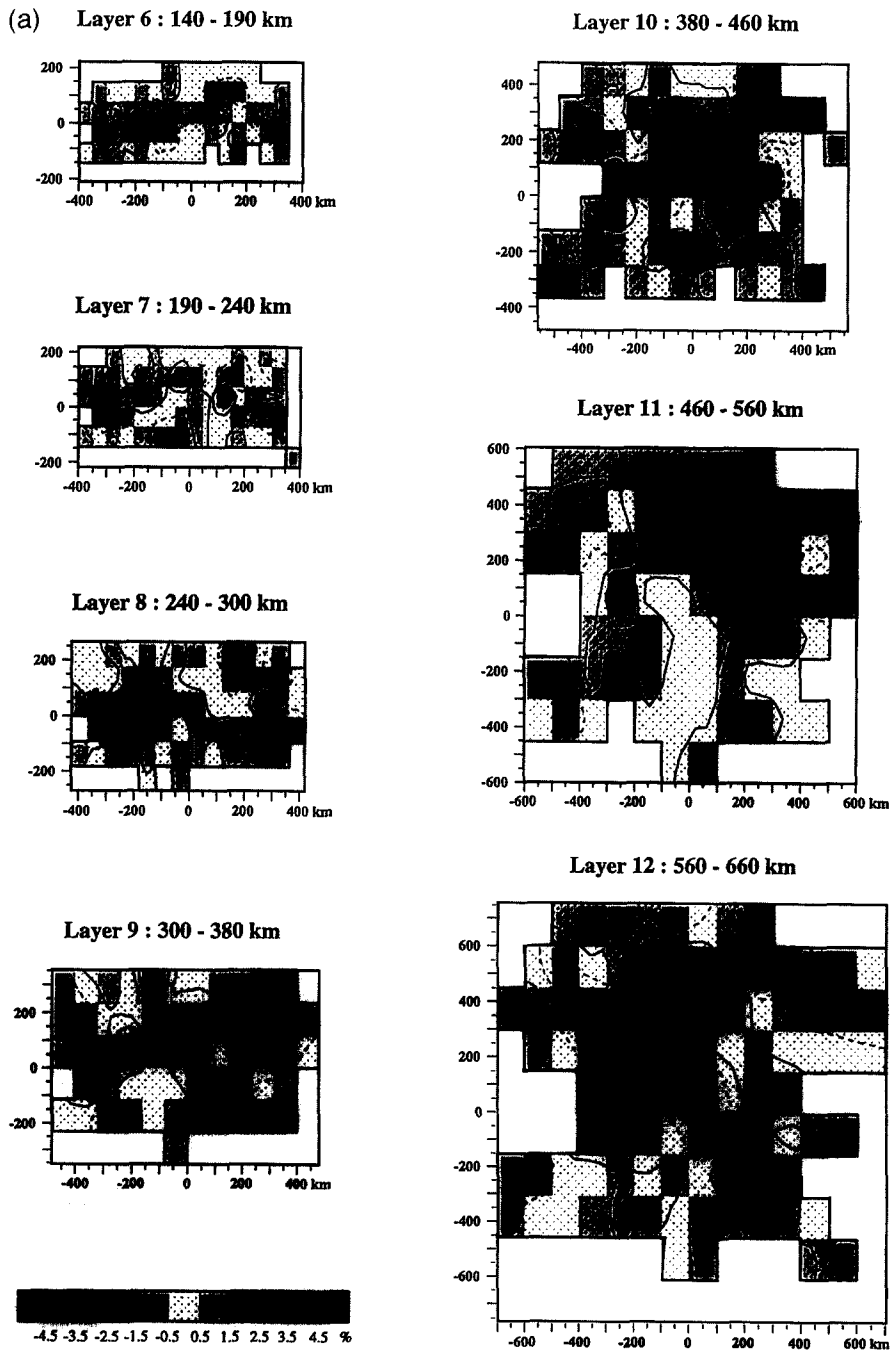


Fig. 4. Velocity perturbations (in %) in the layers below 140 km. The regions with higher velocities than the reference model (positive perturbations) are filled with dotted grey patterns. (a) Original block model resulting from the inversion of teleseismic travel-time residuals, on which iso-perturbation contours have been superimposed. (b) Smoothed perturbation model, together with the seismicity associated with the slab as reported by the NEIS for the past years 20 (black dots). The June 9, 1994 Bolivian earthquake is shown by a larger white dot on Layer 12.

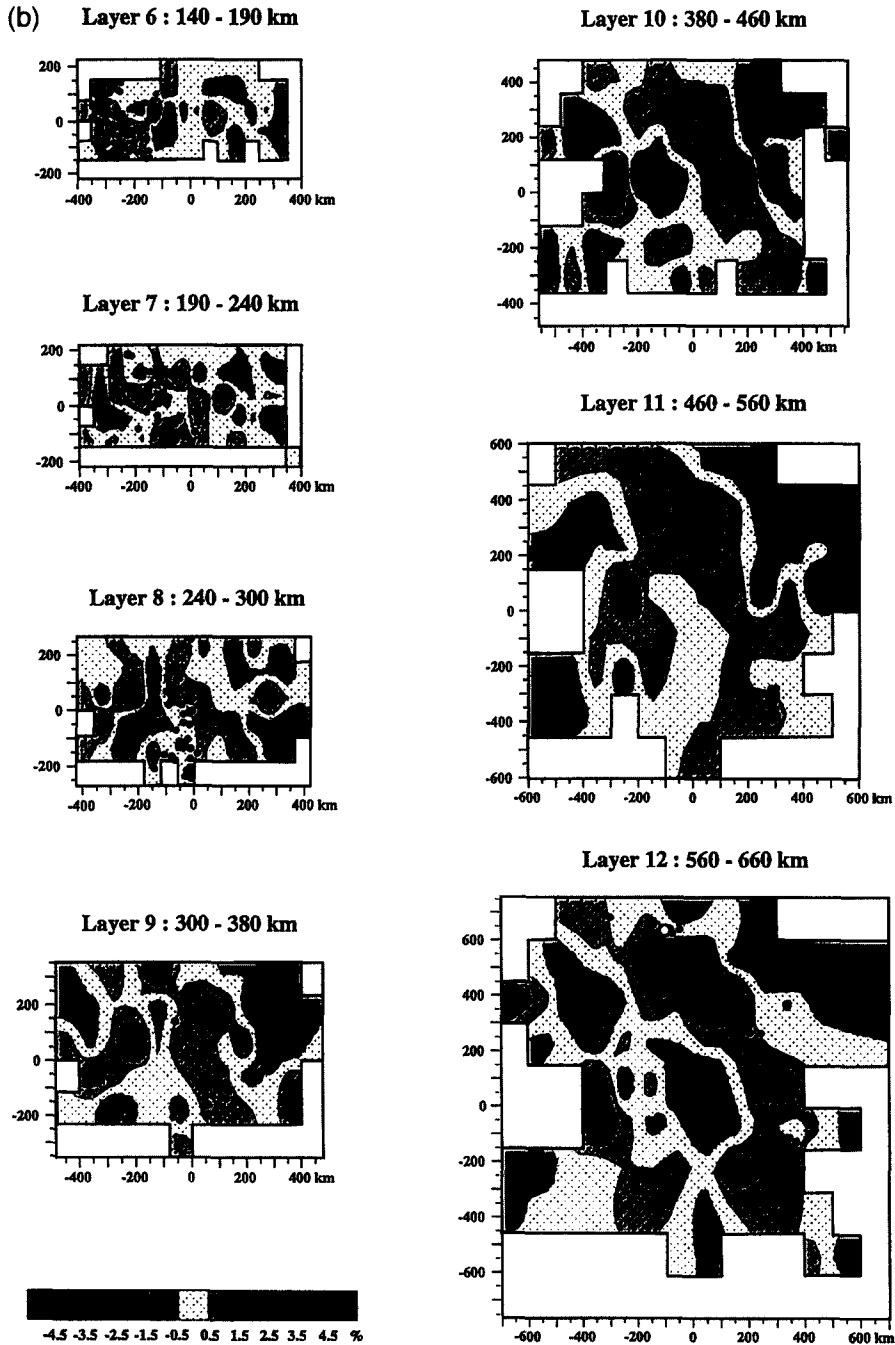


Fig. 4 (continued).

variation reaches 4 s, twice that observed for other azimuths. Such large-scale differences emphasize at the same time that the anomalous structures are deep

and that the region sampled by the rays is far from the axial symmetry. This assertion has to be sustained by the tomography.

3. Inversion

The travel-time residuals are inverted using a version modified by Evans and Achauer (1993) of the 'ACH' inversion method (Aki et al., 1977), extensively described in published literature. The parameterization of the initial velocity model is presented in Table 1 and in Fig. 3. In order to obtain a satisfactory explanation of our data, there is a large reduction in the data variance, we were led to build a 3-D thick initial model. In effect, the reduction of the variance is less than 50% for a 2-D 420-km-thick model; it goes up to 73% for a 3-D model of the same thickness, and reaches 82% when we use a 3-D 660-km-thick model. Therefore, our initial model includes the complete upper mantle and the transition region down to the 650-km discontinuity.

In this paper we will focus on the final velocity perturbations in the mantle below 140 km. Above this depth, the slab, evidenced by the Wadati Benioff zone, is situated at the western extremity of the model, where the resolution is the lowest. On the other hand, beneath 140 km, the slab is well inside the model and resolved. The value of the diagonal element of the resolution matrix for the seven deeper layers is presented in Fig. 3 together with the number of rays in the blocks. We only kept the blocks crossed by more than ten rays. Whatever the depth, the central part of the layers, crossed by numerous rays with varying paths, is the best resolved.

A complementary method with which to check the validity of the final velocity model is to examine how far it explains the observed data. We present in Fig. 2 (grey solid line) the variations along the profile of P-wave residuals computed with the final model for the selected hypocentral regions. We notice a very close correspondence between the observed and computed residuals. The only marked difference is seen at the western extremity of the north-eastern profile, where the divergence reaches 0.4 s. The strong azimuthal variations observed in our data set are satisfactorily explained by the velocity perturbation model obtained by the inversion.

We present in Fig. 4 two images of the velocity perturbations obtained for the seven deepest layers of our model: the original velocity perturbations in blocks in Fig. 4(a), and the smoothed image of the perturbations in Fig. 4(b). The origin of the coordi-

nates is the centre of our parameterized model, that is 19.5°S, 66.5°W. The seismicity reported by the National Earthquake Information Service for the time period 1974–1994 in the respective depth intervals is superimposed on each layer in Fig. 4(b). The largest deep earthquake (June 9, 1994, $M_w = 8.3$, depth = 630 km) instrumentally recorded in Bolivia has been particularized.

Down to 325 km, the Wadati Benioff zone defines the position of the slab in the layers, and is more or less clearly associated with a higher velocity zone. From 140 to 240 km (Layers 6 and 7), the relation between the seismicity and the velocity is not straightforward. Between 240 and 300 km (Layer 8), the subducted plate is displayed by a higher velocity band, underlined by the seismicity, which crosses the layer striking about N160°E. The same velocity structure is observed in Layer 9, associated with the few events which indicate the maximum extent in depth of the Wadati Benioff zone. In Layer 10, the seismic quiescence is total but an elongated higher velocity structure, which clearly prolongates the one observed in the previous layers, is displayed. Finally, we observe again in Layers 11 and 12, down to 660 km, this band of positive anomaly in which the scarce deep seismicity takes place.

In the northern part of Layer 10, the high velocity structure seems to change its trend and become more oblique to the west. The lateral extension of both deeper layers allows the confirmation of this change in orientation of the positive anomaly, which is particularly clear at the 560–660 km depth. Finally, whatever the depth, the velocity contrast associated with the higher velocity zone is weak and seldom exceeds 2.5%.

4. Discussion

The images obtained by teleseismic tomography provide **strong supportive evidence** for the continuity of the slab over regions with gaps in seismicity. The close spacing of the temporary seismic stations together with the good distance–azimuth coverage of the seismic sources allow us to image with high resolution the subducting Nazca plate down to the lower mantle discontinuity. From 240 to 660 km depth, the slab is evidenced by a laterally continuous

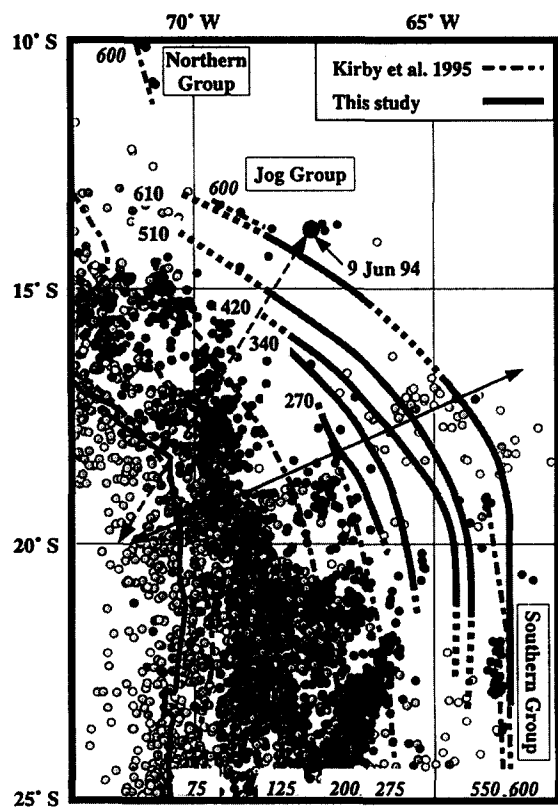


Fig. 5. Comparative study of the subducted Nazca Plate in the Arica Elbow. The seismicity of the Wadati Benioff zone reported by the NEIS is plotted for the time period 1974–1994. The darker the dots, the deeper the hypocentres. The dashed contours to depth are from the updated catalogue of Kirby et al. (1995), as well as the terminology of the deep earthquake groups. The grey contours have been obtained from the tomography, by assigning the maximum of the positive perturbation related to the slab in each layer to its mean depth (solid line where the resolution is higher than 0.4, dotted line where it is lower than 0.4). The arrow ended lines show the location of the two cross-sections presented in Fig. 6.

high-velocity structure, clearly displaying a pronounced bend in the deepest layers of our final model. In the larger scale study by Engdahl et al. (1995), the positive velocity anomaly associated with the slab in the Arica Elbow for the same depth range was of the same order of magnitude but parcelled out. Nevertheless, the interpretation made by these authors also displays a bend in the trace of this higher velocity structure in the transition zone.

We present in Fig. 5 a schematization of the slab geometry deduced from Fig. 4. For every layer in which the slab is clearly identified by higher veloci-

ties, we have drawn a contour passing through the maximum of the positive anomaly. Doing so, we approximate the position of the slab at the mean depth of the layer. In the regions where the resolution is lower than 0.4, the contour is represented by a dotted line. In the same figure, we have reported the seismicity of the NEIS for the past 20 years and the iso-depth contours obtained by Kirby et al. (1995). As the seismicity of slabs is concentrated in the upper part of the subducting lithosphere, there is not an exact correspondence between the iso-depth contours obtained for the maximum velocity contrast and for the seismicity. Nevertheless, the theoretical difference between both contours is well within the uncertainties of their positions, and we may compare them directly. Our 270-km contour is very short and does not fit well with the 275-km contour, the deepest of the Wadati Benioff zone. On the other hand, our 610-km contour is in good spatial agreement with the 600 km depth events. It presents the same strike as the southern group at 22–23°S as well as the ‘jog group’ at 13–14°S, and connects with a smooth bend the well-defined linear trend of these two seismic groups.

The June 9, 1994 Bolivian earthquake occurred in the ‘jog group’ which includes mostly big shocks and has a scarce seismicity. This group is characterized by a WNW strike and a dip about 60° to NNE (Kirby et al., 1995). The main shock and 89 aftershocks were recorded by local permanent and portable instruments, and their spatial and temporal aspect was studied by Myers et al. (1995). These authors show that the deep seismicity can be fitted by a smoothly bent slab, which is clearly compatible with our tomographic image. The aftershock sequence was located with high precision; it defines a slab striking N68°W and dipping 45°NE, which is consistent with the seismicity being confined within the downward extension of the subducted plate.

Therefore, the precise location and shape of the subducted Nazca plate at 560–660 km depth defined by the tomography is fully consistent with the results inferred by previous studies on the deep seismicity. In addition, tomography provides information on the dip of the slab throughout the seismically quiescent zone. Our network layout allows us to sample only a roof-shaped zone aligned on the seismic profile and consequently the north–south extension of the layers

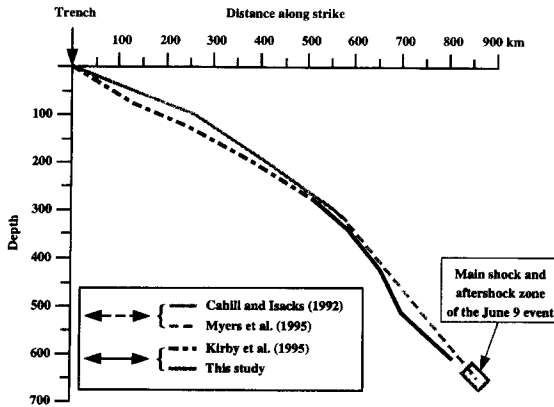


Fig. 6. Profiles through the subducted Nazca Plate. Their location is shown in Fig. 5. The northern profile (dashed line in Fig. 5) is taken from Myers et al. (1995); in its aseismic part, the slab is inferred from Cahill and Isacks (1992) contours. The southern profile (solid line in Fig. 5) is drawn from Kirby et al. (1995) down to the end of the Wadati Benioff zone, and from this study underneath.

depends on their depth. It is therefore not possible to draw from our tomography a vertical cross-section of the slab passing through the 1994 earthquake zone (cf. Fig. 5).

We present in Fig. 6 two cross-sections of the slab in the Arica Elbow obtained by different methods. Their location is reported in Fig. 5 on the map view. The northern one, striking N30°E (dashed line on Fig. 5, grey line on Fig. 6), is extracted from the Myers et al. (1995) paper. The southern one, striking N65°E (solid line on Fig. 5, black line on Fig. 6), is directly deduced from Fig. 5, and is a compilation of the Kirby et al. (1995) contours in the seismically active part of the slab and of the contours deduced from our tomography underneath. On both profiles we observe that the dip of the slab changes with depth. On the northern profile, the dip of the slab increases with depth; it is interpolated from the intermediate depth seismicity down to the June 1994 shock zone, with a 45° mean dip. On the southern profile, from the trench to a depth of 275 km, the seismicity defines an approximately 30° dipping slab; then the dip, inferred from the tomography, increases to more than 50° in the aseismic part of the slab. Finally, the dip decreases to about 40° where the deep seismicity is present, suggesting a deflection of the slab at the bottom of the upper mantle.

When only hypocentral locations are considered, the hypothesis of the continuity of the slab infers in any case that the dip of the slab increases in the aseismic part. Yet Kirby et al. (1995) observe that the deepest events in the 'Southern group' (Fig. 5) are deflected eastward. In this zone, the tomographic images of Engdahl et al. (1995) display a broad region of recumbent slab in the transition zone as well as regions of high-velocity material beneath the 660-km discontinuity. Both studies interpreted these observations by a partial deflection of the slab in the transition zone before continuing into the lower mantle. In contrast, apparent broadening but no deflection of the velocity anomaly occurs on Engdahl's images, at the bottom of the transition zone in the source region of the June 9 event. On the other hand, the constant spacing of the 510- and 610-km contours in Fig. 5 suggests that the deflection of the slab observed on our cross-section should exist in the whole region of the Arica Elbow.

After the Grand (1994) large-scale study, the Engdahl et al. (1995) tomography displays clear evidence of the penetration of the slab in the lower mantle. Kirby and Engdahl interpret the differences that they observe of the velocity anomalies between the two regions of deep earthquakes ('Jog Group' and 'Southern Group') by differences in the level of resistance to penetration into the lower mantle. The vertical extent of our tomography does not allow us to image the lower mantle and consequently to be argumentative on this penetration in itself. Nevertheless, the shape of the slab, as it is defined by the high-velocity body on our tomography, does not suggest any difference in the penetration process along the bend in the Arica Elbow.

Finally, the geometry of the deep slab in the transition zone of southern Peru is still an open question. If it is relatively easy to connect our 610-km contour with the Northern Group through a reverse bend, the closing up of the 200- and the 510-km contours at about 15°S involves a steepening of the slab. Therefore, the transition, from the 50° dip of the aseismic part of the slab deduced from the tomography, to the 70° dip inferred by the James and Snoke (1990) study beneath Peru, seems to occur in this region of the Arica Elbow, and implies a very complicated geometry of the slab between 13°S and 18°S.

Acknowledgements

I would like to thank Anne Paul, Georges Poupinet, and every participant of the Lithoscope Andean Experiment (U. Achauer, M. Aldunate, T. Bianchi, J.P. Caminade, V. Farra, R. Fontanilla, M. Fornari, R. Guiguet, J. Guilbert, B. Guillier, G. Herquel, M. Lambert, C. Martinez, F. Masson, T. Monfret, C. Péquegnat, P. Soler and G. Wittlinger) and Bob Engdahl for helpful review and discussion. This project was sponsored by ORSTOM and INSU-CNRS.

References

- Aki, K., Christofferson, A. and Husebye, E.S., 1977. Determination of the three-dimensional seismic structure of the lithosphere. *J. Geophys. Res.*, 82: 277–296.
- Barazangi, M. and Isacks, B.L., 1976. Spatial distribution of earthquakes and subduction of the Nazca Plate beneath South America. *Geology*, 4: 686–692.
- Barazangi, M. and Isacks, B.L., 1979. Subduction of the Nazca plate beneath Peru: evidence from spatial distribution of earthquakes. *Geophys. J.R. Astr. Soc.*, 57: 537–555.
- Bevis, M. and Isacks, B.L., 1984. Hypocentral trend surface analysis: probing the geometry of Benioff Zones. *J. Geophys. Res.*, 89: 6153–6170.
- Boyd, T.M., Snoke, J.A., Sacks, I.S. and Rodriguez, A.B., 1984. High resolution determination of the Benioff zone geometry beneath southern Peru. *Bull. Seismol. Soc. Am.*, 74: 559–568.
- Cahill, T. and Isacks, B.L., 1992. Seismicity and shape of the subducted Nazca plate. *J. Geophys. Res.*, 97: 17503–17529.
- Comte, D. and Suarez, G., 1995. Stress distribution and geometry of the subducting Nazca plate in northern Chile using teleseismically recorded earthquakes. *Geophys. J. Int.*, 122: 419–440.
- Delouis, B., Cisternas, A., Dorbath, L., Rivera, L. and Kausel, E., 1995. The Andean subduction zone between 22°S and 25°S (Northern Chile): precise geometry and state of stress. *Tectonophys.*, in press.
- Dorbath, C., Paul, A. and the Lithoscope Andean Group, 1996. A tomography of the Andean crust and mantle at 20°S: first results of the Lithoscope experiment. *Phys. Earth Planet. Inter.*, accepted.
- Engdahl, E.R., Van der Hilst, R.D. and Berrocal, J., 1995. Imaging of subducted lithosphere beneath South America. *Geophys. Res. Lett.*, 22: 2317–2320.
- Engbretson, D.C. and Kirby, S.H., 1992. Deep Nazca slab seismicity: why is it so anomalous? *Eos, Trans. Am. Geophys. Un.*, 73(43): 379.
- Evans, J.R. and Achauer, U., 1993. Teleseismic velocity tomography using the ACH method: theory and application to continental scale studies. In: H.M. Iyer and K. Hirahara (Editors), *Seismic Tomography*. Chapman and Hall, London, pp. 319–360.
- Grand, S., 1994. Mantle shear structure beneath the Americas and surrounding oceans. *J. Geophys. Res.*, 99: 11591–11621.
- Grange, F., Cunningham, P., Gagnepain, J., Hatzfeld, D., Molnar, P., Ocola, L., Rodrigues, A., Roecker, S.W., Stock, J.M. and Suarez, G., 1984. The configuration of the seismic zone and the downgoing slab in southern Peru. *J. Geophys. Res.*, 11: 38–41.
- Harris, R.A., Iyer, H.M. and Dawson, P.B., 1991. Imaging the Juan de Fuca Plate beneath Southern Oregon using teleseismic P wave residuals. *J. Geophys. Res.*, 96: 19879–19889.
- Herrin, E., 1968. Seismological tables for P phases. *Bull. Seismol. Soc. Am.*, 58: 1193–1242.
- Hirahara, K., 1981. Three-dimensional seismic structure beneath southwest Japan: the subducting Philippine Sea plate. *Tectonophys.*, 79: 1–44.
- Hirahara, K. and Hasemi, A., 1993. Tomography of subduction zones using local and regional earthquakes and teleseisms. In: H.M. Iyer and K. Hirahara (Editors), *Seismic Tomography*. Chapman and Hall, London, pp. 519–562.
- Isacks, B.L. and Barazangi, M., 1973. High-frequency shear waves guided by a continuous lithosphere descending beneath western South America. *Geophys. J.R. Astron. Soc.*, 33: 129–139.
- James, D.E. and Snoke, J.A., 1990. Seismic evidence for continuity of the deep slab beneath central and eastern Peru. *J. Geophys. Res.*, 95: 4989–5001.
- Jordan, T.E., Isacks, B.L., Allmendinger, R.W., Brewer, J.A., Ramos, V.A. and Ando, C.J., 1983. Andean tectonics related to geometry of subducted Nazca plate. *Geol. Soc. Am. Bull.*, 94: 341–361.
- Kirby, S.H., Okal, E.A. and Engdahl, E.R., 1995. The June 9, 1994, Bolivian deep earthquake: an exceptional event in an extraordinary subduction zone. *Geophys. Res. Lett.*, 22: 2233–2236.
- Myers, S.M., Wallace, T.C., Beck, S.L., Silver, P.G., Zandt, G., Vandecar, J. and Minaya, E., 1995. Implications of spatial and temporal development of the aftershock sequence for the Mw 8.3 June 9, 1994 deep Bolivian earthquake. *Geophys. Res. Lett.*, 22: 2269–2272.
- Snoke, J.A., Sack, I.S. and Okada, H., 1974. Empirical models for anomalous high-frequency arrivals from deep-focus earthquakes in South America. *Geophys. J. R. Astron. Soc.*, 37: 133–139.
- Stauder, W., 1973. Mechanisms and spatial distribution of Chilean earthquakes with relation to subduction of the oceanic plate. *J. Geophys. Res.*, 78: 5033–5061.
- Stauder, W., 1975. Subduction of the Nazca plate under Peru as evidenced by focal mechanisms and by seismicity. *J. Geophys. Res.*, 80: 1053–1064.
- Sykes, L. and Hayes, D., 1971. Seismicity and tectonics of South America and adjacent oceanic areas. *Geol. Soc. Am. Programs, Cordilleran section*, 3: 206.
- Wortel, R., 1982. Seismicity and rheology of subducted slabs. *Nature*, 296: 553–556.
- Wortel, M.J.R., 1984. Spatial and temporal variations in the Andean subduction zone. *J. Geol. Soc. Lond.*, 141: 783–791.